LiM 2011

# Microchannels Direct Machining using the Femtosecond Smooth Ablation Method

Machado*, L. M., Samad, R. E., Freitas, A. Z., Vieira Jr., N. D., de Rossi, W.

*Center for Lasers and Applications – IPEN-CNEN/SP, Av. Prof. Lineu Prestes 2242, Cidade Universitária, São Paulo SP, 05508-000, Brazil*

**Abstract**

Damage threshold and ablation rate measurements were performed on Bk7 glass for femtosecond single and multipulses. The incubation parameter was found and used to develop a new strategy for machining microchannels in Bk7. Optical Coherent Tomography - OCT measurements showed that this ablation process can be effective in obtaining deep, well defined square cross section microchannels with no cracks or resolidified material. It was also verified that OCT can be useful in detecting small index refraction changes induced to the surround of the machined area.

*Keywords:* femtosencond; microchannels; geometrical path; micromachining

## 1. Introduction

Microfluidic technology now enables the production of smaller and more accurate microfluidic chemical and biological devices, allowing different applications ranging from DNA analyzers [1] to micro chemical reactors [2]. Usually, these microchannels are fabricated in transparent materials to allow actuators and optical sensor integration, and in this case, the most common fabrication method is lithography. Other developmental methods use different kinds of laser for direct writing ablation [3, 4], or irradiation followed by chemical etching [5]. In direct laser ablation, IR to UV nanosecond pulses have been used to create microstructures, but they generally lead to cracks or heat affected zones. Femtosecond laser ablation is considered a better alternative process to machining for such transparent materials. This is because the high intensities guarantee greater efficiency of the nonlinear absorption process, permitting a deterministic ablation process in which high definition and extremely low heat affected zones are possible.

Machining of cavities in Bk7, for example, requires multipulse irradiation, to remove the necessary amount of material. This, means that an incubation effect takes place, which must be taken into consideration. This effect is characterized by a lowering of the ablation threshold induced by previous irradiated pulses [6], which must be considered in order to ensure better control of the ablation process. In this context, this study sought to create microchannels in Bk7, of dimensions and shape that comply with the requirements of microfluidic devices in terms

---

of cross section, finishing and heat-affected zone. A machining strategy was established, resulting in production of microchannels with controlled dimensions, greater depth, and sharp edges and without dross or burrs.

## 2. Experimental procedure

The experimental setup, shown in Figure 1, used a femtosecond Ti:sapphire laser system based on the Chirped Pulse Amplification method (Rainbow-Femtopower oscillator-amplifier). The laser beam, with wavelength centered in 800 nm, pulse length of 55 fs, and diameter of 6 mm, was focused on the sample surface through a 38 mm focal length. The intensity profile was Gaussian with a $M^2$ factor equal to 1.4. The beam was linearly polarized, allowing simple energy adjustment by means of a half-wave plate combined with a Glan-Thompson polarizer. A two axis coordinate system with micrometric accuracy and CNC programming was used to guide the sample through a pre-defined path. A piece of Schott's borosilicate crown glass, $\lambda/10$ plain, was used to create a series of microchannels and to create ablation for the threshold measurements.

All samples were cleaned in the same way, with acetone in ultrasound, for tree minutes, and dried with optical tissue to eliminate any residue. The ablation threshold measurements were performed using the diameter-regression technique [7] for single and multipulses, and their values were estimated by the relation between the average fluence and the square diameter of the ablated area. Thus, a large set of irradiations were performed on the surface of the glass, by varying the laser pulse energy and the number of overlapped shots. For each energy value and spatial pulse overlap, a total of six different damage conditions were created, ranging from 2.4 to 7.5 J/cm² for unique and overlapped pulses. The diameter of the ablated area was measured with an optical microscope, and the volume of the ablated material was measured using a VEECO® optical profiler. The ablation thresholds measured for different numbers of overlapping pulses allowed the evaluation of the incubation parameter for this glass, which was then used to establish a machining strategy for microchannels production. The shape and morphological details of these channels were observed by means of Optical Coherent Tomography – OCT, Scanning Electronic Microscopy – SEM and optical microscopy.
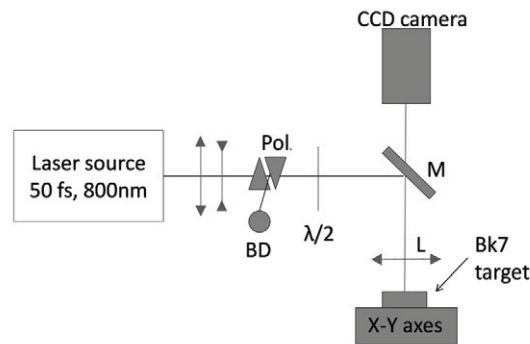


Figure 1. Schematic diagram of the experimental setup for femtosecond machining. L: lens $f$ = 38mm lens; Pol.: Glan Thompson polarizer; M: mirror; BD: beam dump

## 3. Results and Discussion

The damage threshold is related to the lowest fluence $F_{th}$ needed to initiate the ablation process, due to a single laser shot. However, when two or more pulses are placed together (one over the other), damage can occur at considerably lower energies. This is due to an "incubation phenomenon" [8, 9] whereby information from preceding irradiations is retained, causing "pre-damage" in the dielectric material, locally altering the crystal lattice structure, and generating inter-band levels, which makes multi-photonic absorption much more likely. This previous damage cannot be seen directly, and may include vacancies, color centers or self-trapped excitons [10]. When milling a cavity, many laser shots must be overlapped to obtain the desired depth, and in this case, a knowledge of the incubation factor is of primary importance and must be taken into consideration.

## 3.1. Ablation threshold

The damage threshold $F_{th}$ can be experimentally obtained through the relation between laser pulse average fluence, $F_0^{AV}$, and diameter D of the damage produced by it. This relation was first proposed to map the intensity distribution of 20 ps laser pulses [7] based on the fact that the size of the ablated region is dependent on the fluence used. It was also shown that this same relation is valid when overlapped pulses are applied to the sample surface [11]. The equation below represents the relation between the laser pulse fluence $F_0^{AV}$ and diameter D of the ablated area:

$$F_0^{AV} = F_{th}^N \exp\left(\frac{D^2}{2\omega_0^2}\right)$$
(1)

Where,

$$F_0^{AV} = \frac{E_{pulse}}{\pi\omega_0^2},$$
(2)

$E_{pulse}$ is the individual pulse energy and $\omega_0$ is the beam radius on the surface of the sample. The damage threshold for $N$ superimposed pulses, $F_{th}^N$, is constant and in the first approximation, depends only on the material type.

Equation 1 is then used to obtain $F_{th}^N$ by plotting the experimental values of $F_0^{AV}$ x $D^2$ in a semi-log graph as shown in Figure 2. Values of $F_0^{AV}$ were firstly evaluated through equation 2, where $\omega_0$ (9.1 µm) was obtained by the equation:

$$\phi_{focus.} = 4M^2 \lambda f / (\pi. \phi_0)$$
(3)

where $\phi_{focus.} = 2\omega_0$ is the focused beam diameter, $\lambda$ is the central laser wavelength, $f$ is the lens focal length and $\phi_0$ is the beam diameter before the focusing lens. This $\omega_0$ value is further replaced by the one evaluated from the plot of equation 1. This procedure [8] enables the "real" $\omega_0$ to be recovered, which is more accurate than the one obtained from equation 3. The corrected value of $\omega_0$ (now $\omega_0 = 6.7$ µm) is then used to recalculate the fluencies used, and to obtain the corrected damage threshold. Figure 2 shows the relation between the corrected average fluence for single shots as a function of square diameter of the damage. Adjustment of equation 1 gives a value of $2.3 \pm 0.7$ J/cm$^2$ as single shot damage threshold for BK7, similar to others seen elsewhere [8, 9].

The behavior of damage threshold as function of number of overlapped pulses $F_{th}(N)$ can be described by the empirically developed equation established by A. Rosenfeld et al. [6, 9]. It is assured when using the same wavelength and energy for all laser pulses:

$$F_{th}(N) = F_{th}(\infty) + [F_{th}(1) - F_{th}(\infty)]e^{-k(N-1)}$$
(4)

Where $F_{th}(1)$ and $F_{th}(\infty)$ are damage thresholds for one and infinite pulses respectively. $k$ is an empirical parameter, independent of $N$ in first approximation, that characterize the material sensibility for the buildup of defects and the photon absorption increases. The higher the k value, the less pulses are needed to reach saturation point in the damage threshold, i. e., $F_{th}(N) \approx F_{th}(\infty)$. The incubation factor $k$ can be obtained by adjusting equation 3 and using experimental data for $F_{th}(N)$ x $N$. The $k$ value obtained was $0.73 \pm 0.23$, which can be used to calculate $F_{th}(N)$ for any $N$ value.

Damage threshold measurements as a function of $N$ are shown in the plot in Figure 3 and show a significant decrease in $F_{th}$ as $N$ increases. For $N$=1.024 pulses, $F_{th}$ is 4 times smaller than $F_{th}(N=1)$. 3D geometric profiles of damaged surfaces (Figure 4b) were obtained by means of an optical profiler, and were used to calculate the ablated volume as a function of energy for several different $N$ values of laser shots. The results, shown in Figure 4a, highlight the significant influence of pulse overlap on the ablated volume. The amount of ablated material is greatly increased as the $N$ number of laser shots increases, and this can be used when milling large and deep channels as in

the case of some microfluidic devices. These insights give us a useful tool for estimating the erosion rate for a given processing condition, and selecting the best machining strategy.
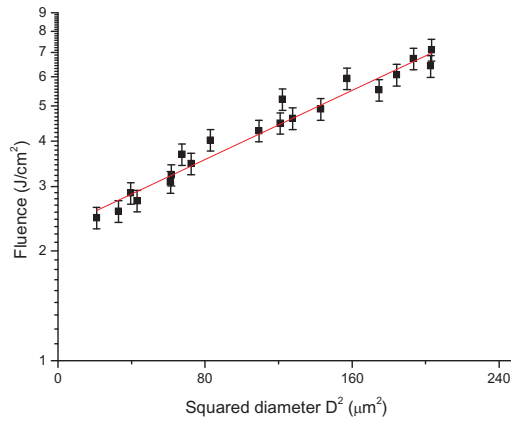


Figure 2. Corrected laser fluence vs. square diameter of damage. $D^2$ represents the average value for 6 single laser shots, and the error bars show the amplitude of standard deviation. The damage threshold $F_{th}$ is obtained through linear interpolation for $D^2=0$.
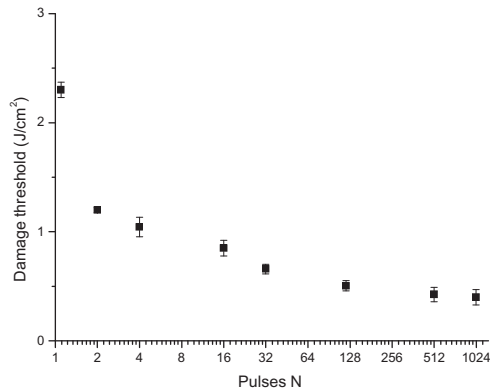


Figure 3. Damage threshold vs. number of overlapped pulses. The error bars show the amplitude of standard deviation.
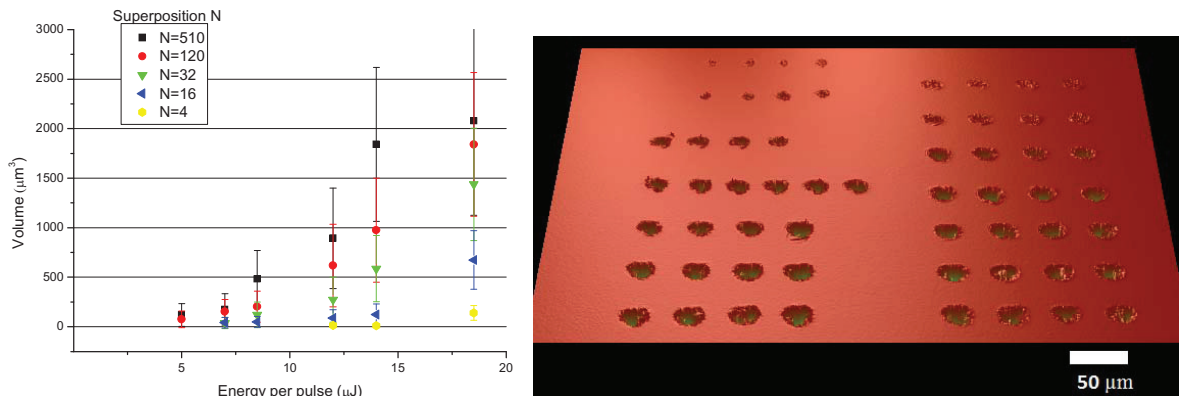


Figure 4. (a) Ablated volume as a function of pulse energy and overlapping *N;* (b) 3D view of array of damage used to calculate the extracted volume.

## 3.2. Machining Strategies

It is clear that not only are laser parameters important in processing, but also the response and susceptibility of the material to these parameters, which depend on the previous irradiation of its surface. Hence, the efficiency of the ablation and state of the final surface may differ considerably, depending on the machining parameters used. Furthermore, the surface response is constantly changing as the machining proceeds. The challenge, therefore, is not only to choose between high intensity with low pulse overlap, and low intensity with a high degree of overlap, but also to adapt the laser parameters to the changes that occur in the surface properties. To solve this problem, two machining strategies were established: A direct, harder one, with high intensity and high overlapping of pulses, and a smoother one, where the scanning speed is considerably increased and overlapping of pulses are consequently decreased. The second condition covers the surface with a smaller number of shots in each overlay, making it necessary to repeat the process many times, in order to reach the desired depth.

In both strategies, several parallel lines were swept by the laser focused spot along to the channel track, as shown in Figure 5. The parameters subjected to variation were:

- Longitudinal pulse overlap,
- Lateral displacement of the pulses,
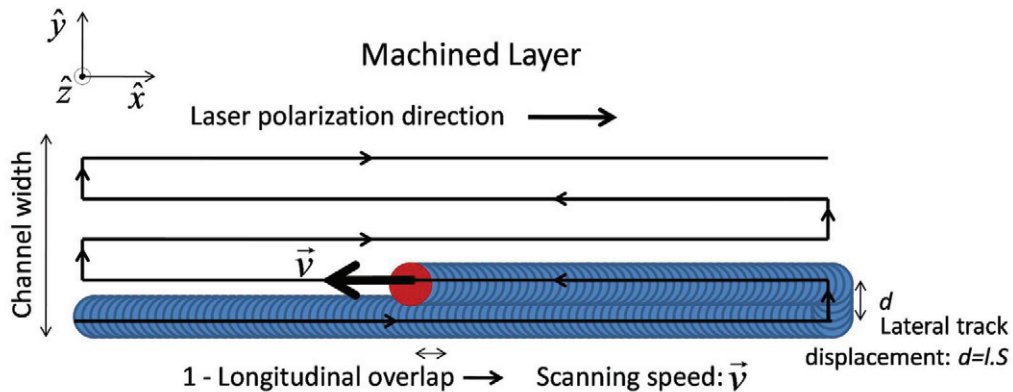- Pulse energy.



Figure 5. Schematic diagram of the focus path for one machined layer. Beam polarization and scanning direction are parallel to the long axis of the channel. Variables were scanning speed $\vec{v}$, pulse energy $E_{pulse}$ and lateral displacement $d$.

## 3.3. Hard machining

The first approach was to improve efficiency by ablating a large amount of material per pulse. To do this, high intensity (energy) and high overlapping laser shots were used. Energy and longitudinal pulse overlap were kept constant for each machining condition, and were $N=500$ and $E_{pulse}=33\mu J$, corresponding to 22 J/cm$^2$. To obtain a projected final width of 100 µm, parallel arrays of tracks were machined choosing four different lateral distances "$d$" between the centers of the tracks for each condition: $d = 10, 20, 30$ and $40$ µm.

The number $N$ of longitudinal overlapped pulses was obtained through the relation involving beam scanning speed "$V$", spot diameter "$\phi_{focus}$" and repetition rate "$T$":

$$N = (\phi_{focus}.T)/V \tag{5}$$

With a repetition rate of $T = 1.000$ Hz, the scanning speed was kept constant at 1.6 mm/min.

Although uniform, these irradiation conditions lead to shallow (60 µm), asymmetric and irregular channels. OCT images of transversal sections of these tracks, Figure 6, also show a very deep and tapered whitish region below the

machined surface. This region is not related to catastrophic damage, and cannot be directly seen with an optical microscopy. In reality this region had its index of refraction permanently changed by nonlinear effects induced by the high intensity of the pulses[10, 11]. Besides the poor geometric result, the Figure 6 shows that part of pulse energy is being lost by a deep transmission to the bulk of the material. This behavior seems to be related to the incubation effects mentioned above. As the sequence of pulses overlaps, the difference between the intensities used (and fixed) and the damage threshold intensity becomes larger, and the effect on the material becomes more severe. Besides inducing nonlinear effects that focus the beam deeper below the surface, the high amount of ablated material also produces a skewed wall for each individual track. The slope of the machined track reflects the laser pulses of the adjacent track that follows it, making the ablated area erratic and unpredictable, Figure 7.
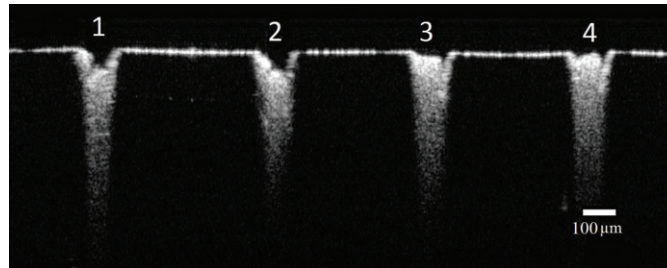


Figure 6. Cross section OCT image of channels machined with "hard machining". The displacements between adjacent tracks are $d$=10, 20, 30, and 40 µm for channels from 1 to 4 respectively. $N = 500$ and $E_{pulse} = 33$ µJ.
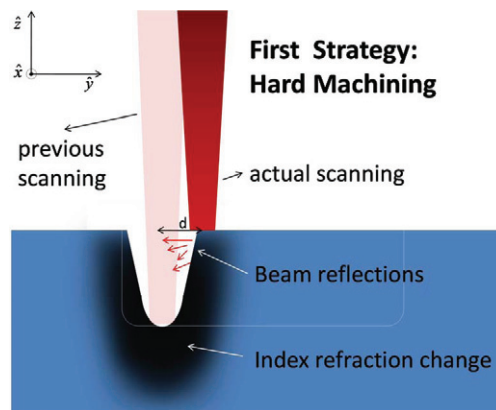


Figure 7. Schematic diagram of the hard machining strategy. Longitudinal overlapping is high enough to obtain a greater depth in just one machined layer.

### 3.4. Smooth machining

The beam scanning procedure shown in Figure 5 was adopted in this approach. However, in this case, some modifications were implemented. The longitudinal overlap was lowered, and the lateral overlap was evaluated in accordance with track width, predicted by the incubation parameter $k$. As $N$ is lower, the volume ablated in each overlay of pulses is not enough to obtain a deep channel, requiring several sequences of layers to be machined (Figure 8). The total number of layers was four, and for each one, the incubated effects caused by previous machining were taken into account. The distance between adjacent tracks was evaluated based on the predicted track width "$S$" (that was being machined) and was therefore adjusted for each new layer. The value of "$S$" was derived from equations 2 and 3, and can be written as:

$$S(N, F_0^{AV}) \equiv \omega_0 \sqrt{2 \ln\left(\frac{F_0^{AV}}{F_{th}(N)}\right)} = D \qquad (6)$$

Equation 4 gives the value of the track width as function of $N$ and average fluence of the laser pulses $F_0^{AV}$. Lateral displacement of the tracks "$d$" is a fraction of "$S$" according to the desired overlap "$l$" (see Figure 5). Therefore, $d = S.l$, where $0 < l < 1$, and in all cases $l$ was fixed at 0.8 corresponding to 20% of lateral overlap.

In the first layer, $N = 4$ was chosen as longitudinal overlap, and lateral displacement was evaluated according to $d = l.S(N=4, F_0^{AV})$. In the second layer, scanning speed was modified to correspond to $N = 12$, where the $D$ and $S$ values were calculated for $N=16$, since these 12 shots are overlapped on the 4 preceding ones. The same procedure was used for the next two layers, with $N=32$ and $N=128$ (accumulated shots). The process stopped at N=128, since the incubation effect seems to be stabilized from this point (Figure 3).

Figure 9 shows the OCT image of some machined channels, where the above-described strategy was adopted. Two different energies were used, and for each one, channels were produced for $N=4$; $N=16$; $N=32$ and $N=128$. Energy of 10 µJ led to a very shallow Figure, even for $N=128$, whereas energy of 33 µJ resulted in much deeper channel. There was a clear improvement in the shape of the channels; the cross section shows a flat bottom and a straight wall, almost perpendicular to the surface. Figure 10 shows the SEM image of a channel machined with this strategy, where it is possible to see a well-defined edge without dross, burr or any resolidified material attached.

Adjusting the diameter of the damage resulting from previous irradiations keeps the lateral overlap constant, spreading the amount of pre-damaged material smoothly and homogeneously. When this is not taken into account, deposited energy is more promptly absorbed in places where accumulation of pre-damage is greater, resulting in a non-homogeneous ablation.

A real microfluidic device was produced in BK7 using this strategy, and is shown in Figure 11. Machined channels exhibited a good square cross section of 100 x 100 µm$^2$, with a 100 µm space between the borders.
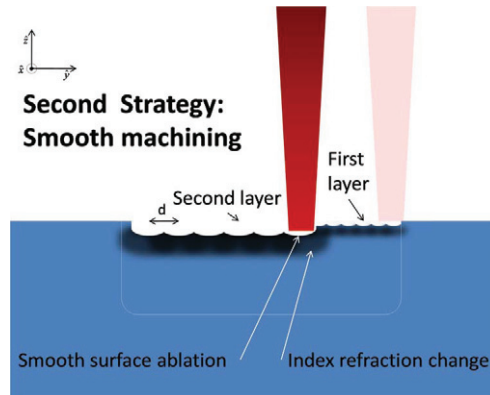


Figure 8. Soft machining strategy, where total depth is achieved by means of several machined layers. In each layer, the longitudinal overlap is changed and the lateral displacement is adjusted to compensate for the change in the dimension of the damage.
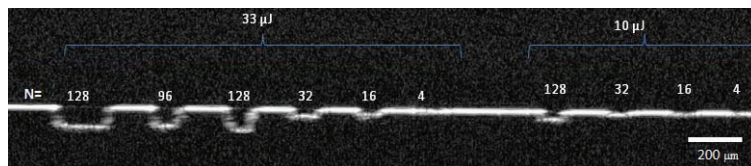


Figure 9. Cross section OCT image of channels machined using the second strategy. The numbers above the channels represent the total number N of overlapped pulses. Pulse energies of 10 µJ and 33 µJ were used. The last channel on the left is 200 µm in width; the others are 100 µm.
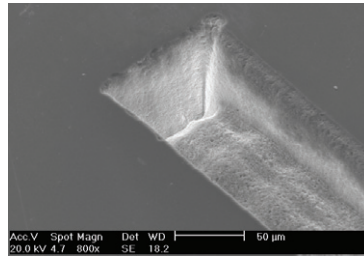
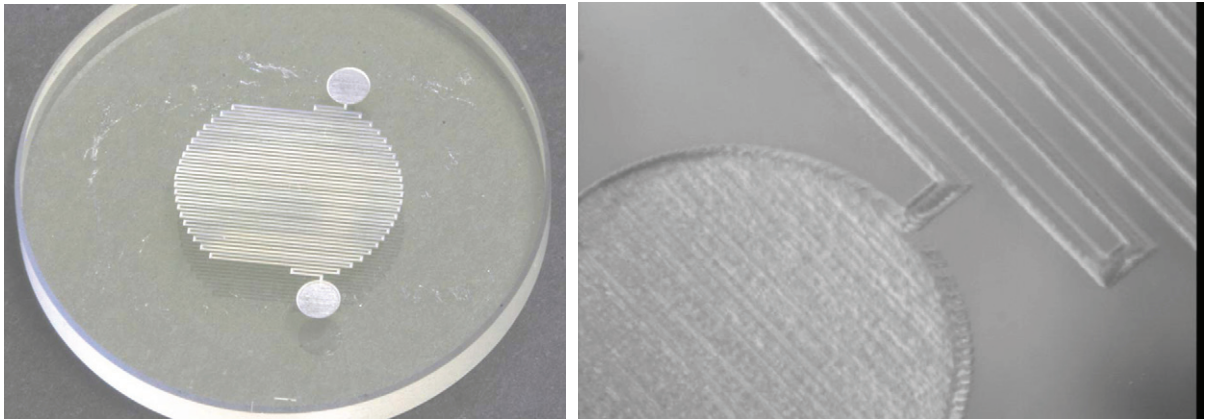Figure 10. SEM image of a microchannel directly machined with the smooth strategy,



Figure 11. Microfluidic device "milled" in BK7 with 46 microchannels 100 x 100 $\mu m^2$ of cross section and 100 $\mu m$ displaced each other.

## 4. Conclusion

This work showed the importance of incubation effects in machining BK7 glass. The same laser pulse intensities can produce very different milled shapes if pre-damage is not taken into account.

A high degree of longitudinal overlap without lateral displacement compensation of the tracks resulted in irregular channels with a deep, conical change in the refractive index distribution below the bottom of the channel.

Good control of the channel shape was achieved when the incubation effect was taken into account in evaluating lateral overlapping. This was done in four steps, adjusting the lateral displacement for each one. Starting with a low longitudinal overlap ($N$=4) and going up to $N$=128, this procedure resulted in channels with good square section, flat bottom, high edge definition, and no attached dross or melted material.

This is a new procedure, as far as we know, and has not yet been mentioned in literature. It can produce pre-defined shapes, and results in a finish that comparable to that obtained by laser ablation followed by chemical etching, with the advantage that it is experimentally easier and faster.

OCT imaging have proven to be a useful tool for microchannel inspection. It is simple, fast and also can detect small index refraction variations in the bulk near the machined region. This can be valuable in choosing the best processing parameters, leading to better efficiency and preventing unwanted effects in adjacent regions.

**Acknowledgements**

**References**

[1] Burns, M.A., et al., An Integrated Nanoliter DNA Analysis Device. Science, 1998. 282(5388): p. 484-487.

[2] Tripathi, A., Microfluidics Reactors for Diagnostic Applications. Annual Review of Biomedical Engineering. 13(1).

[3] Aguilar, C.A., et al., Direct micro-patterning of biodegradable polymers using ultraviolet and femtosecond lasers. Biomaterials, 2005. 26(36): p. 7642-7649.

[4] Sugioka, K., Y. Hanada, and K. Midorikawa, 3D integration of microcomponents in a single glass chip by femtosecond laser direct writing for biochemical analysis. Applied Surface Science, 2007. 253(15): p. 6595-6598.

[5] Vishnubhatla, K.C., Shape control of microchannels fabricated in fused silica by femtosecond laser irradiation and chemical etching. OPTICS EXPRESS, 2009 17(10 ).

[6] Ashkenasi, D., A. Rosenfeld, and R. Stoian. Laser-induced incubation in transparent materials and possible consequences for surface and bulk micro-structuring with ultrashort pulses. in Society of Photo-Optical Instrumentation Engineers (SPIE) Conference Series. 2002.

[7] Liu, J.M., Opt. Lett. , 1982. 7: p. 196.

[8] Sanner, N., et al., Measurement of femtosecond laser-induced damage and ablation thresholds in dielectrics. Applied Physics A: Materials Science & Processing, 2009. 94: p. 889-897.

[9] Ben-Yakar, A. and R.L. Byer, Femtosecond laser ablation properties of borosilicate glass. Journal of Applied Physics, 2004. 96(9): p. 5316-5323.

[10] Taylor, R., et al., Ultra-high resolution index of refraction profiles of femtosecond laser modified silica structures. Opt. Express, 2003. 11(7): p. 775-781.

[11] Saliminia, A., et al., The influence of self-focusing and filamentation on refractive index modifications in fused silica using intense femtosecond pulses. Optics Communications, 2004. 241(4-6): p. 529-538.